Dynamic Behavior of Helicon Wave Produced Plasma

Shinohara, Shunjiro
Department of High Energy Engineering and Sciences, Interdisciplinary Graduate School of Engineering Sciences, Kyushu University

Miyauchi, Yoko
Department of High Energy Engineering and Sciences, Interdisciplinary Graduate School of Engineering Sciences, Kyushu University

Kawai, Yoshinobu
Department of High Energy Engineering and Sciences, Interdisciplinary Graduate School of Engineering Sciences, Kyushu University

https://doi.org/10.15017/17375

出版情報：九州大学大学院総合理工学報告. 17 (2), pp.215-228, 1995-09-01. 九州大学大学院総合理工学研究科
バージョン：
権利関係：

九州大学大学院総合理工学研究科報告
第17巻 第2号 215-228頁 平成7年9月

Engineering Sciences Reports, Kyushu University
(KYUSHU DAIGAKU SOGORIKOGAKU KENKYUKA HOKOKU)
Vol. 17, No. 2, pp. 215-228, SEPT 1995

Dynamic Behavior of Helicon Wave Produced Plasma

Shunjiro SHINOHARA*, Yoko MIYAUCHI** and Yoshinobu KAWAI*

(Received May 31, 1995)

Exciting $m=1$ and -1 helical modes, the dynamic behavior of a helicon wave produced plasma is investigated. The RF (radio frequency) power dependence, antenna-plasma coupling, and time evolution of plasma parameters and Ar line intensities are studied in relation to the density jump, *i. e.*, steep density increase to a level of 10^{13} cm^{-3} by an application of the input RF power more than 1 kW. Before the density jump, the excited wave is localized near the antenna, exhibiting a standing wave character. After the jump, this wave propagates outwards and a dispersion relation of the helicon wave is confirmed.

1. Introduction

A high density plasma production by a helicon wave[1-6] as a high density plasma source has become very attractive in confinement devices as well as in plasma processing ones. It was shown that a high density plasma up to $\geq 10^{13}$ cm^{-3} could by produced efficiently by an application of RF (radio frequency) waves with the axial magnetic field B_0 of more than several hundreds of G. In addition, the helicon wave, satisfying a dispersion relation[3,6] and expected magnetic field distributions[1,4,6], was observed with a spatial decreasing amplitude.

However, it should be stressed that an essential role of plasma production including a plasma initiation by the helicon wave solely, has not been verified up to the present. In relation to this, we have not clarified the "density jump" phenomenon, which is characterized as a steep (abrupt) increase in the plasma density to a level of 10^{13} cm^{-3} with more than a threshold RF power P_{th} of ≤ 1 kW within a time scale of several hundreds of μs.

Moreover, time behavior (especially from the plasma initiation to the established phases) and space structures of plasma parameters including excited wave fields have been scarcely studied, in spite of the active and intensive use of this wave as a plasma production tool, e. g., in the plasma processing field. Needless to say, even the basic database of plasma parameters are not enough. These findings obtained so far are also scraps of information, and the mechanism and behavior of production and sustainment are still open questions to be studied.

For the topic of this machanism, we investigate the dynamic behavior of a helicon wave produced plasma in detail and systematically. Here in this paper, after describing an experimental system in section 2, spatiotempoal plasma parameters (in section 3) and their dependencies on RF power (in section 4) are presented: electron temperature, electron density and ion saturation curent, including antenna plasma resistance (antenna-plasma

*Department of High Energy Engineering Science
**Graduate Student, Department of High Energy Engineering Science

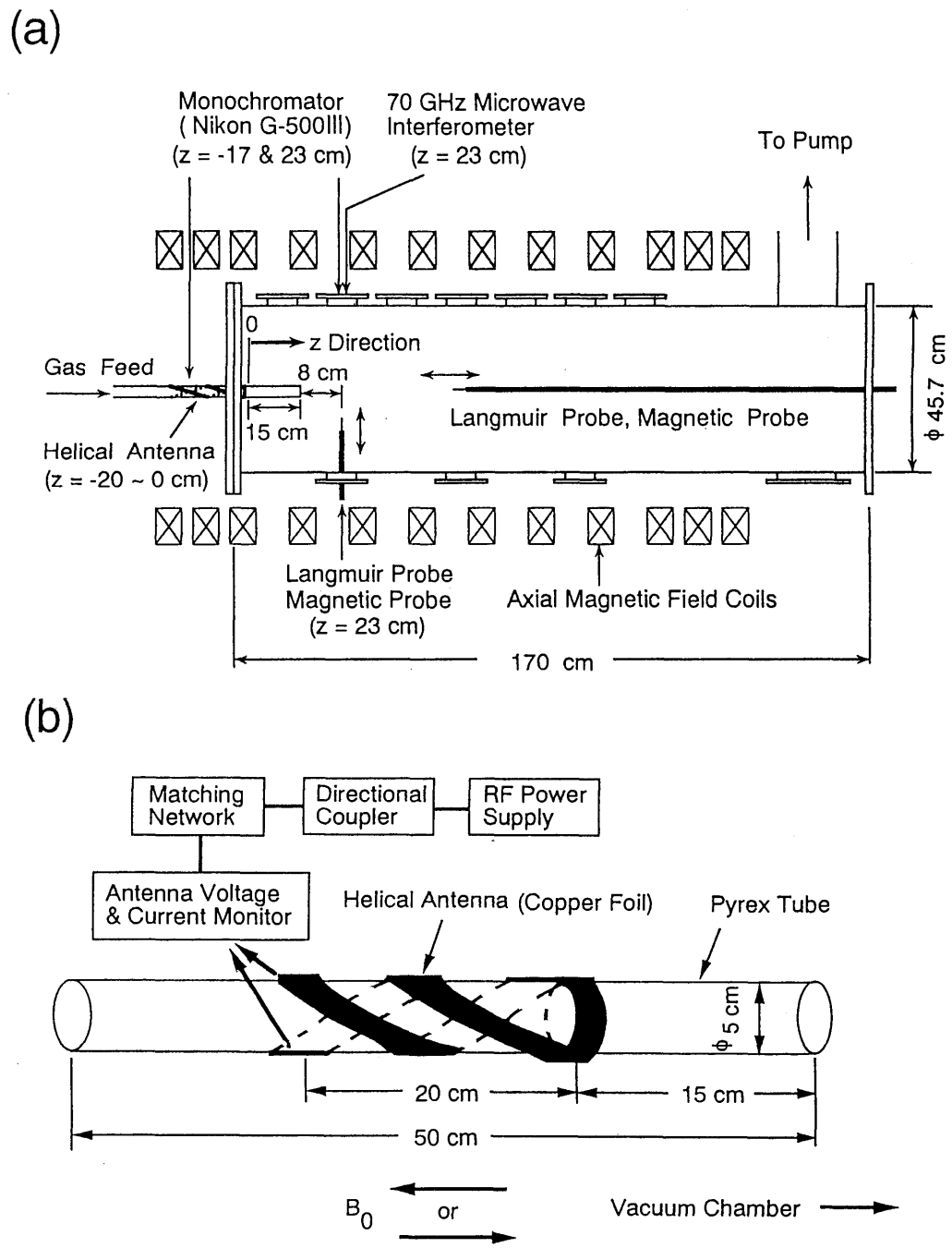

Fig. 1 Schematic views of (a) experimental apparatus and (b) antenna structure including RF system.

coupling) as well as Ar I and Ar II line intensities, are measured. In section 5, the history of the wave character on (ω_p, $k_{//}$) plane (ω_p: plasma angular frequency, $k_{//}$: parallel wave number) at the inside and outside antenna regions, in addition to the wave patterns, is investigated for the first time to analyze the excited wave nature. Finally, conclusions are presented in section 6.

2. Experimental setup

The experimental system is shown in **Fig. 1**. The filling pressure of Ar gas, fed into the left side of the Pyrex tube (inner diameter is 5 cm and total length is 50 cm, axial position of $z=-35\sim15$ cm), is 0.6 mTorr with the static axial magnetic field of $B_0=1$ kG typically. Here, $z=0$ cm is defined at the right side of a helical antenna.

The RF power and frequency are <3 kW and 7 MHz, respectively, and a RF pulse width is 2 ms with a duty of <0.1 for a protection of a thermal damage on the helical antenna and RF system. The RF power supply is connected to the antenna through a directional coupler, which picks up incident and reflected power, *i.e.*, P_{inc} and P_{ref}, a matching box (split tank circuit) and monitors of antenna voltage and current. The antenna length is 20 cm ($z=-20\sim0$ cm) with one turn winding, made of copper foil with 2.5 cm wide and 0.25 cm thick, around a Pyrex tube. Exciting $m=1$ or -1 modes (m: azimuthal mode number) can be selected by changing the sign of the axial magnetic field B_0 in this system. Here, $m=1$ (-1) denotes right−hand (left−hand) rotation with respect to the magnetic field B_0.

Plasma parameters and excited wave fields are measured by movable Langmuir and magnetic probes inserted into the plasma, respectively. A balanced mixer for the interferometric wave measurements, and a boxcar integrator due to a pulse plasma production are used in addition. A 70 GHz microwave interferometer for absolute plasma density measurement and a visible monochromator (focal length is 50 cm) are also installed.

3. Spatiotemporal plasma behavior

Time evolution of n_e (electron density), T_e (electron temperature), Ar I (419.8 nm) and Ar II (488.0 nm) line intensities are shown in **Fig. 2** ($m=1$, $P_{inp}=1.4$ kW (hereafter P_{inp} is defined at $t=1.8$ ms unless denoted)) and **Fig. 3** ($m=-1$, $P_{inp}=1.2$ kW). Here, input RF power P_{inp} is $P_{inc}-P_{ref}$ and net power P_{net} is defined as $(P_{inc}-P_{ref})\times R_p/(R_v+R_p)$, where $R_v(=0.27\ \Omega)$ and R_p are vacuum and plasma loading resistances, respectively (antenna-plasma coupling will be described in section 4). Note that a power reflection coefficient $R=P_{ref}/P_{inc}$ is typically <0.3 at $t>0.5$ ms.

These parameters are measured at the outside ($z=23$ cm by a Langmuir probe and a monochromator) as well as inside ($z=-17$ cm by a monochromator) antenna regions. The electron density n_e measured by Langmuir probes is carefully calibrated by a 70 GHz microwave interferometer, which is important to determine the absolute value (*e.g.*, the influx on the substrate for the plasma aided manufacturing, and a dispersion relation depending on the plasma density), but it has not been used so much up to now.

The electron density n_e is low for about 0.2 ms after an application of RF power, but this density increases suddenly to a level of $>10^{13}$ cm^{-3} (so called "density jump") after

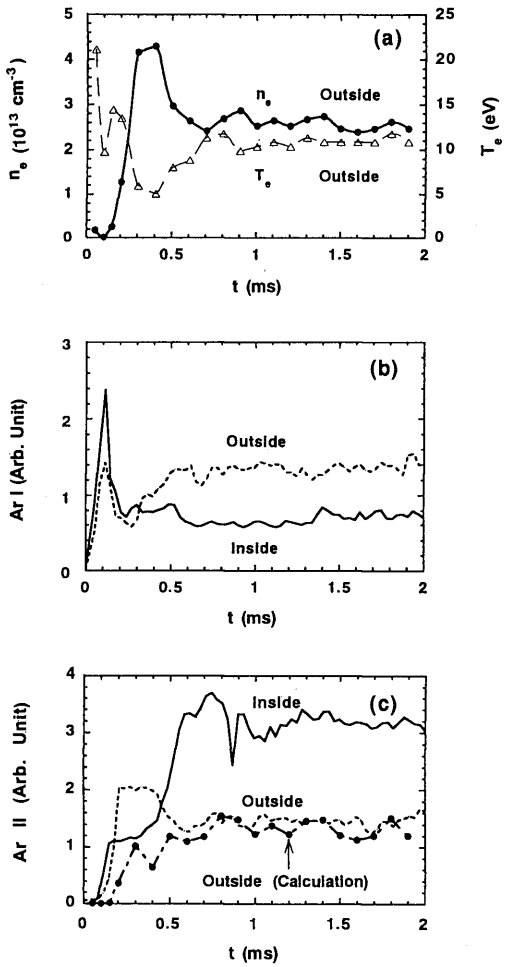

Fig. 2 Time evolution of (a) electron density n_e and electron temperature T_e, (b) Ar I (419.8 nm) and (c) Ar II (488.0 nm) line intensities for $m=1$ excitation.

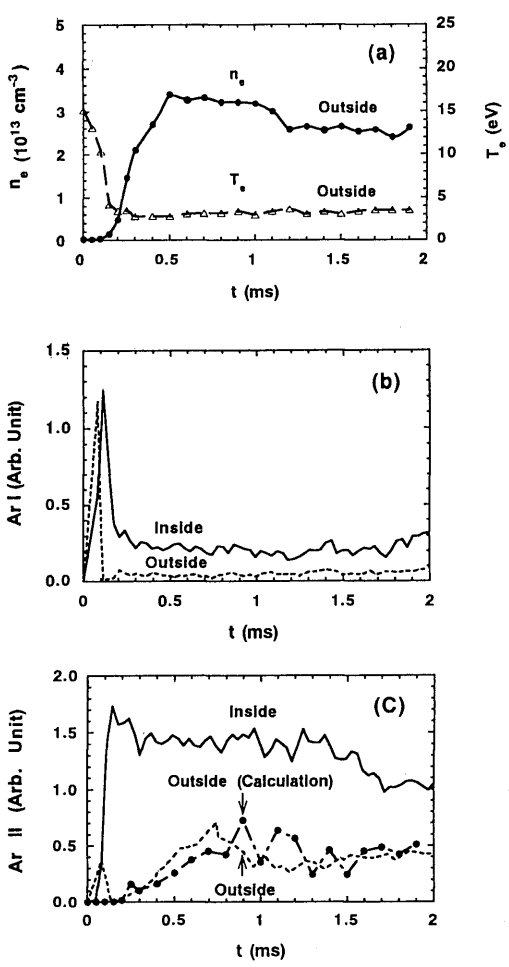

Fig. 3 Time evolution of (a) electron density n_e and electron temperature T_e, (b) Ar I (419.8 nm) and (c) Ar II (488.0 nm) line intensities for $m=-1$ excitation.

that. When P_{inp} is lower than a threshold value P_{th} of about 1 kW, n_e, Ar I and Ar II line intensities remain low during whole 2 ms RF pulse (dependencies of plasma parameters on P_{inp} are shown in **Figs. 8** and **10**). After the density jump with a decrease in the electron temperature, Ar II (Ar I) intensity increases (decreases), which shows a neutral density decrease and a higher ionization rate.

These phenomena obtained are more pronounced for the $m=-1$ case, and the time behaviors of Ar line intensities are similar for $B_0=0.5$ kG case. Note that Ar I (Ar II) intensity is proportional to $n_e\, n_0 < \sigma\, v >_{\mathrm{I}}$ ($n_e\, n_i < \sigma\, v >_{\mathrm{II}}$), where n_0, n_i and σ are neutral density, ion density and cross section, respectively, and $< \sigma\, v >_{\mathrm{I}}$ and $< \sigma\, v >_{\mathrm{II}}$ are functions of the electron temperature, assuming a Maxwellian electron veloity distribution.

For $m=1$ excitation case, relative Ar I and Ar II line intensities at the outside region,

which are normalized by respective intensities at the inside region, are higher than those for $m=-1$ excitation due to the different axial plasma density profile: effective plasma length along the z axis is longer for $m=1$ case as shown in **Fig. 7**.. There is a tendency that the electron temperature T_e at the outside region is higher for $m=1$ excitation than that for $m=-1$ excitation (see **Figs. 2 (a), 3 (a)** and **8 (b)**), and n_e at the antenna region for $m=-1$ excitation is higher than that at the outside region (not shown), which is consistent with a result in **Fig. 7 (b)**.

Time evolution of Ar II line intensity can well be simulated after the plasma establishment, as shown in **Figs. 2 (c)** and **3 (c)**. This intensity, which is proportional to $n_e n_i < \sigma v >_{II}$, is estimated by the use of the experimental values of $n_e (=n_i)$ and T_e, based on the cross section data dependent on T_e[7]. There is a controversy whether high energy electrons (several tens of eV) exist or not[8]. With an increase in the electron temperature from a few eV to several tens of eV, Ar II line intensity increases drastically by more than two orders of magnitude from calculation[7]. The experimental and calculated results suggest that even if exists, there is a small portion of high electron energy component (more than 10 eV). On the contrary, the number of high energy electrons may be somewhat larger at the plasma formation phase, since a small hump of this Ar II intensity can be seen.

Figure 4 shows changes of ion saturation (radial) current profiles I_{is} at the outside region ($z=23$ cm) with time for (a) $m=1$ ($P_{inp}=2.2$ kW) and (b) $m=-1$ ($P_{inp}=1.6$kW) excitation. As is seen, I_{is} small and broad before the density jump. Then I_{is} becomes large abruptly after the jump, but the this profile for the $m=-1$ case is more peaked than that for the $m=1$ case. This can also be found from the n_e measurements ($z=23$ cm) in **Figs. 5 (a)** ($P_{inp}=1.7$ kW, $m=1$) and **6 (a)** ($P_{inp}=1.4$ kW, $m=-1$).

The more peaked profile for the $m=-1$ case may reflect that the effect of the heating profile is stronger than the diffusion effect; Radial profile of the energy dissipation term of $<E_z * j_z>$ (sum of the z components of the excited electric field and currnet) due to the collisional damping, is expected to be more peaked for

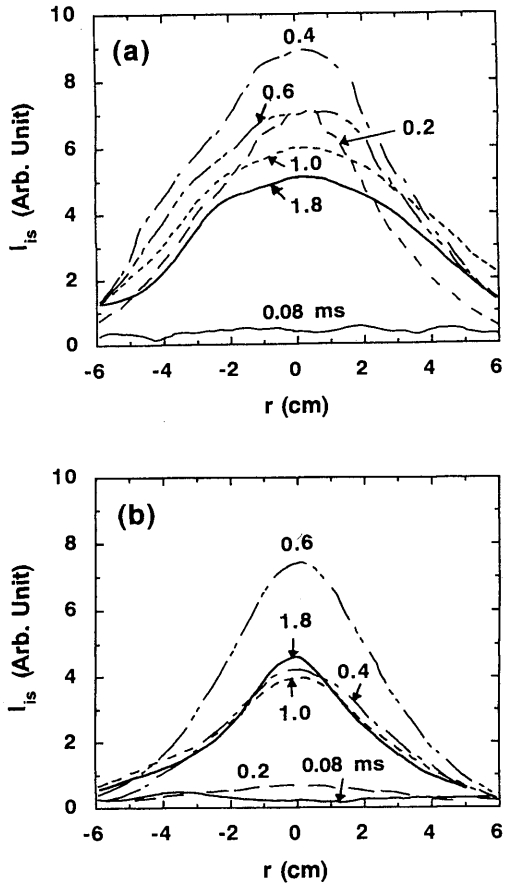

Fig. 4 Time evolution of radial profiles of ion saturation current I_{is} for (a) $m=1$ and (b) $m=-1$ excitation at $z=23$ cm.

the $m=-1$ case[4,5], *i. e.*, near the peak of the z component of the excited magnetic field B_z. Therefore, a narrow dense profile for $m=-1$ excitation and a broad, uniform profile for $m=1$ can be expected according to Ref. 5. On the contrary, the wave induced radial transport is worse for the $m=-1$ case than that for $m=1$ case[9], but it has not been so much discussed quantitatively.

Here, global energy confinement time is several tens of μs under our experimental conditions. Although an experimental diffusion has not been explained quantitatively by theories up to now in the straight magnetic field configuration, an axial energy confinement time (ambipolar diffusion) is estimated to be greater than 100 μs, which is smaller than the radial one by a factor of few times. Note that the parallel (along the magnetic field line) transit time through the plasma by the ion sound speed is ≥ 100 μs.

Therefore, even though the radial diffusion due to the excited wave is altered by the sign of m, this contribution may be smaller than the heating profile effect. Needless to say, effects of anomalous diffusion and another azimuthal mode such as $m=0$ and higher radial mode (see Eq. (35) in Ref. 2) must be taken into account in addition, to interpret the obtained profile quantitatively. As the density profile is also governed by the neutral density near the outer plasma region, further studies (such as confinement and excited wave field measurements) are needed to understand this profile difference.

Figures 5 (a) and **6 (a)** show that the electron temperature T_e is nearly constant (gradually decreases with the plasma radius) and higher (lower) for the $m=1$ ($m=-1$)

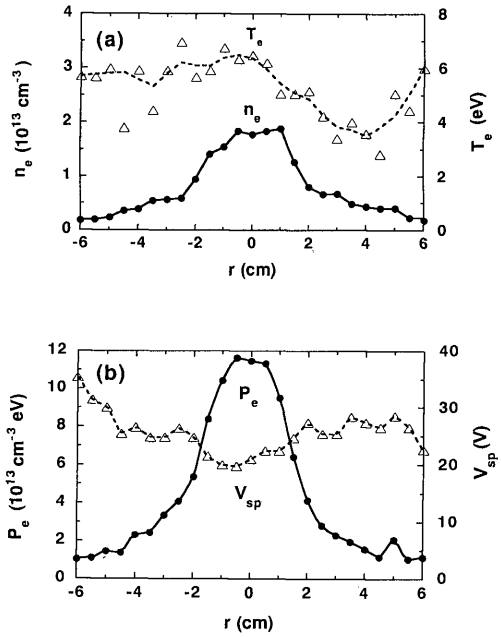

Fig. 5 Radial profiles of (a) electron temperature T_e and density n_e, and (b) electron pressure $P_e \equiv n_e\, k\, T_e$ and space potential V_{sp} for $m=1$ excitation at $z=23$ cm.

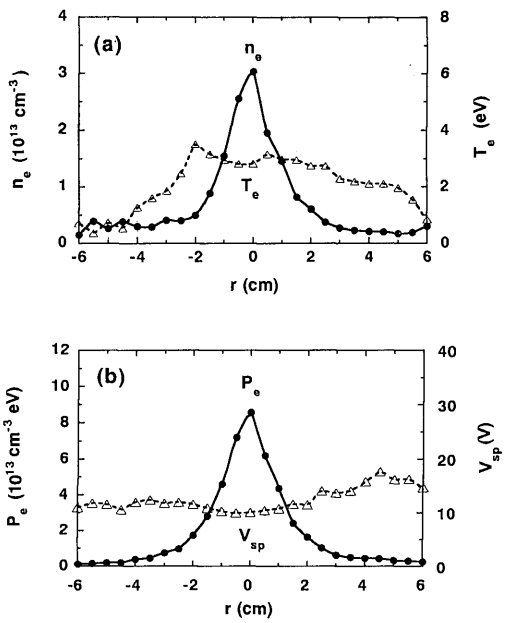

Fig. 6 Radial profiles of (a) electron temperature T_e and density n_e, and (b) electron pressure $P_e \equiv n_e\, k\, T_e$ and space potential V_{sp} for $m=-1$ excitation at $z=23$ cm.

case. In **Figs. 5 (b)** and **6 (b)**, an electron pressure $P_e \equiv n_e\, k\, T_e$ (k: Boltzmann constant) is also more peaked for the $m=-1$ case (see **Figs. 4, 5 (a)** and **6 (a)**) with the lower space potential V_{sp} compared with the $m=1$ case.

Figure 7 shows time evolution of the axial profiles of ion saturation current I_{is} for (a) $m=1$ ($P_{inp}=1.1$ kW) and (b) $m=-1$ ($P_{inp}=1.2$ kW) excitation, measured at the plasma center of $r=0$ cm. At the early stage after the density jump for the $m=1$ case, I_{is} is peaked near the antenna region, then the peak position moves outwards (positive z direction) with time. Previous results with the lower RF power shows that n_e and I_{is} (T_e) increase (decreases) with z position ($z < 50$ cm) at the later stage of the plasma establishment with almost constant electron pressure P_e along the z axis. For the higher RF power case, I_{is} and P_e gradually decrease with z position (20 cm$<z<$60 cm region).

For the $m=-1$ case on the contrary, the peak of I_{is} is localized near the antenna region and I_{is} decreases with an increase in the positive z position (a slight profile change with time). This localization of I_{is} may come from a larger collisional damping due to the higher plasma density near the antenna.

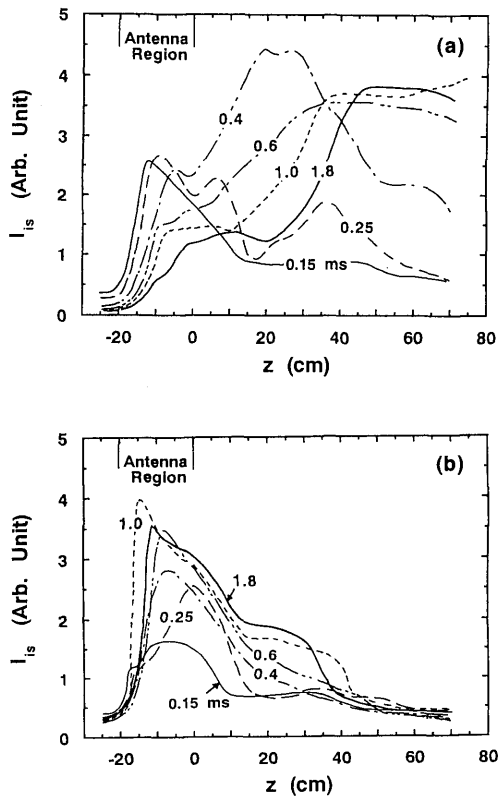

Fig. 7 Time evolution of axial profiles of ion saturation current I_{is} for (a) $m=1$ and (b) $m=-1$ excitation at $r=0$ cm.

4. Power dependence

In this section, a relationship between plasma parameters and input power P_{inp} is presented. **Figure 8** shows dependencies of n_e and T_e, at the outside ($z=23$ cm) antenna region of $r=0$ cm, on input RF power P_{inp} for the $m=1$ and -1 excitation. When P_{inp} is greater than a threshold power P_{th} of about 1kW, an electron density jump by three orders of magnitude (from an order of 10^{10} cm^{-3} to that of 10^{13} cm^{-3}) with a drop of the electron temperature (from 10−15 eV to 3−8 eV ranges) is found, *i. e.*, a clear discontinuity of the electron density at P_{inp} is near P_{th} (see a bold arrow with impedance matching in **Fig. 8 (a)**). There is no appreciable difference of P_{th} between the $m=1$ and -1 excitation for this density jump.

In the high density region (after the jump), n_e changes little even though P_{inp} is further increased, which implies a saturation of the ionization, *i. e.*, nearly fully ionization for the fixed filling pressure (the same trend of a saturation of Ar II line intensity is found in **Fig. 10**). In this high density region, T_e at the outside region ($m=1$) and n_e at the inside region ($m=-1$) are higher than other cases by a factor of less than 3.

In this experiment as stated before, a power reflection coefficient $R = P_{ref}/P_{inc}$ is typically <

0.3 at $t > 0.5$ ms for both high and low plasma densities by adjusting the capacitance values in the matching box. Needless to say, R is high at the initial stage (before the density jump) of the RF pulse for the high power case of $P_{inp} > P_{th}$, although R is low after the density jump at the later stage. If we keep capacitance values in the matching box constant and increasing RF power from a low value (R is also low), n_e increases drastically near $P_{inp} = P_{th}$ but P_{inp} suddenly becomes low due to a mismatching (a large reflection of $R > 0.5$), whose trajectory is depicted in **Fig. 8 (a)** (see a double-line arrow without an impedance matching and crosses for large R case ($m=1$)). Here, both P_{inp} of about 1kW (just before the density jump) and about 0.5 kW (the lowest data of crosses in **Fig. 8** after the jump) correspond to $P_{net} = P_{inp} \times R_p/(R_v + R_p)$ of about 0.4 kW. For this large reflection case, only $P_{inp} > 0.5$ kW is necessary to have high density plasma but distorted electric fields exist due to this large R. This suggests that a high electric field, especially near field effect (inductive field), is also important to have high density plasma as well as generating the initial plasma.

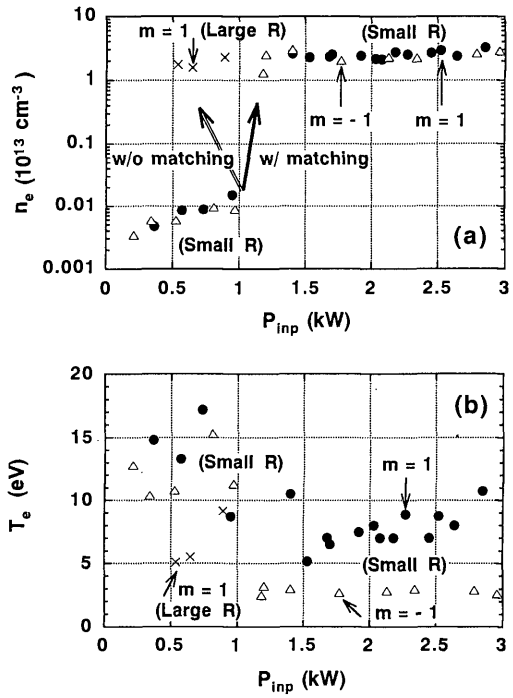

Fig. 8 Dependencies of (a) electron density n_e and (b) electron temperature T_e on input RF power P_{inp} for $m=1$ and -1 excitation at $z = 23$ cm. Here, closed circles, open triangles and crosses represent excitation of $m = 1$, $m = -1$, and $m = 1$ with a large reflection $R = P_{ref}/P_{inc}$, respectively. A bold arrow shows a trajectory with unchanged low R by adjusting matching circuit values (with impedance matching), and a double-line arrow shows that from small R to large R without changing circuit values (without impedance matching), near the density jump region.

Antenna-plasma coupling is studied by changing RF power P_{inp}. Before a density jump of $P_{inp} < P_{th}$, plasma loading resistance R_p is low about 0.2 Ω ($\leq$ vacuum loading of R_v). This R_p increases drastically after the density jump, and then nearly constant with P_{inp} (same feature with a obtained relationship between n_e and P_{inp} in **Fig. 8 (a)**). This shows a good coupling efficiency $\eta = R_p/(R_v + R_p)$ of about 0.9 for high density region, and also means a lowering of the RF applied voltage on the antenna in the presence of this high density plasma (desirable for reducing the direct accerelation of the charged particles near the antenna, which is critically important for the material processing). The total inductance of the antenna including the feeder part during experiments is about 0.4 μH, which differs little between cases with and without plasma (and also regardless of the plasma density).

Next, plasma loading resistance R_p is studied as a function of the plasma density n_e near the antenna position ($r=0$ cm and $z=-5$ cm), because R_p is considered to depend mainly

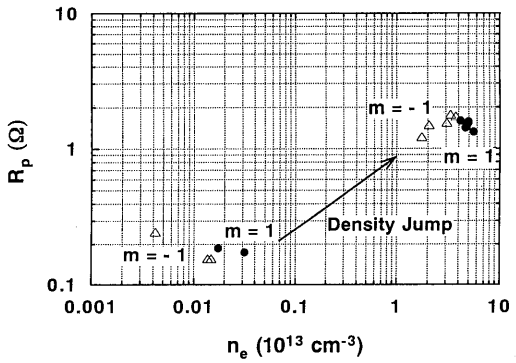

Fig. 9 Dependence of plasma loading resistance R_p on plasma density n_e (antenna region). Here, closed circles and open triangles denote cases of $m = 1$ and $m = -1$ excitation, respectively.

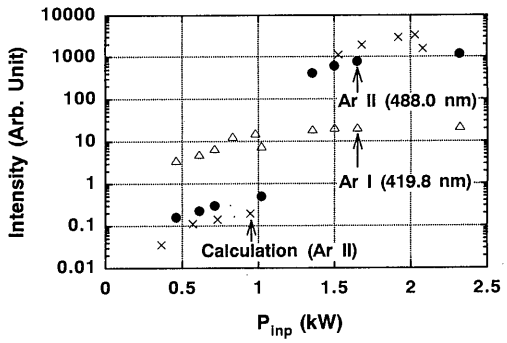

Fig. 10 Ar I (419.8 nm) and Ar II (488.0 nm) line intensities vs. input RF power P_{inp} for $m=1$ excitation at $z=23$ cm. Here, open triangles, closed circles and crosses represent experimental line intensities of Ar I, Ar II and calculation line intensity of Ar II, respectively.

on the local plasma density facing the antenna (see **Fig. 9**). As R_p and n_e behave similarly with P_{inp} mentioned above, R_p is low (about 0.2 Ω) before the density jump ($P_{inp}<P_{th}$) and becomes higher (1−2 Ω) by nearly one order of magnitude after that ($P_{inp}>P_{th}$). In each region of low and high densities, R_p is weakly dependent on n_e and there is a slight different dependence between the $m=1$ and -1 cases.

This obtained value of R_p after the density jump shows a comparative or somewhat stronger plasma coupling normalized by the antenna size length and width, compared with a fast magnetosonic wave[10,11] and an ion Bernstein wave[11,12] in the ion cyclotron range of frequency (ICRF) in a small tokamak TNT-A. Comparing the experimental plasma conditions, the central electron temperature (density) for the present case is lower (higher) than that of those waves by one order of magnitude (a few times). This leads to the higher collision frequency by two orders of magnitude with the smaller plasma cross section by one order of magnitude (than the previous ICRF experiments in the TNT-A machine).

Dependencies of Ar I (419.8 nm) and Ar II (488.0 nm) line intensities on the input power P_{inp} are shown in **Fig. 10** for $m=1$ excitation at the outside ($z=23$ cm) antenna region. After the density jump, Ar II intensity increases by more than two orders of magnitude, whereas Ar I intensity increases a little (similar results are obtained for the $m=-1$ excitation case). When a large reflection ($R>0.5$) data after the density jump are added, a similar trajectory (like a double-line arrow in **Fig. 8 (a)**) can also be obtained. The dependence of Ar II intensity on P_{inp} is also consistent with calculation (the same procedure described in section 3) results.

5. Time evolution of wave structures

The history of the excited wave feature is studied on (ω_p, $k_{//}$) plane to check the dispersion relation, as shown in **Figs. 11 (a)** ($m=1$) and **11 (b)** ($m=-1$) with $P_{inp}=1.9$ kW. Here, the $k_{//}$ value, averaged over 0.5 −1 wavelength along the z axis ($r=0$ cm), is

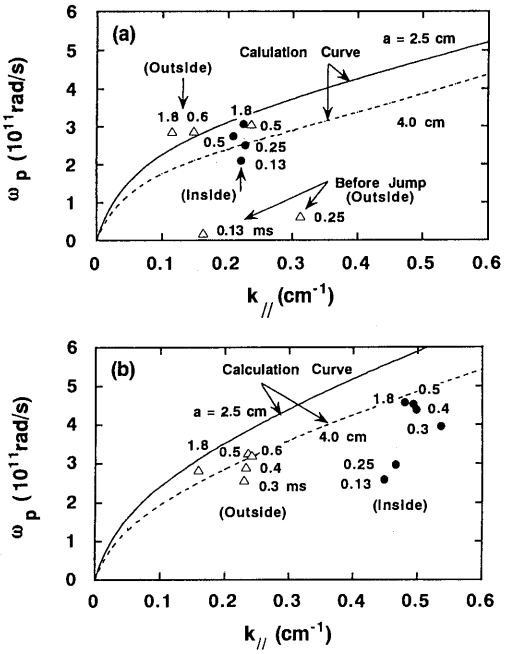

Fig. 11 History of the dispersion relation on (plasma frequency, parallel wave number) = (ω_p, $k_{//}$) plane for (a) $m=1$ and (b) $m=-1$ excitation at $r=0$ cm. Here, closed circles and open triangles show cases measured at the inside and outside antenna regions, respectively.

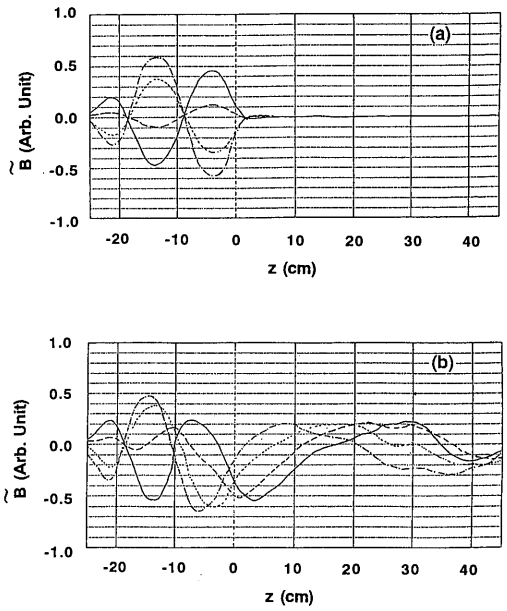

Fig. 12 Typical wave patterns of excited perpendicular magnetic field at (a) $t=0.03$ ms and (b) $t=1.8$ ms for $m=1$ excitation at $r=0$ cm. Here, solid, broken, dotted and chain lines represent cases of phase $\Delta\phi=0$, -0.21π, -0.42π and -0.66π, respectively.

determined by the magnetic probe signal using the interferometric method with the antenna current. Here, the antenna excited fundamental $k_{//}$ value in the vacuum $k_{//a}$ is 0.31 cm^{-1}. The plasma density n_e used to calculate ω_p is measured at $z=-5$ cm (inside) and 23 cm (outside), and $\omega_p=1.8\times10^{11}$ rad/s corresponds to $n_e=10^{13}$ cm^{-3}.

In this figure, two calculation curves of a (plasma radius) $=2.5$ cm and 4 cm cases are drawn, taking the first radial mode in Eq. (35)[2]. Experimentally a is about 2.5 cm at the inside of the antenna region and ≥ 2.5 cm at the outside of it: the effective plasma radii at the outside region are about 3 cm for $m=1$ excitation and 2.5 cm for $m=-1$ (see **Figs. 5 (a)** and **6 (a)**), neglecting slopes at the larger radii.

Before the density jump, a wave does not propagate to the outer side of the antenna region so much (see **Fig. 12 (a)**). The dispersion relation of the helicon wave, whose wave is a whistler wave with boundary conditions[2], is not satisfied at the outside region (see $t=0.13$ and 0.25 ms is **Fig. 11 (a)**). This can also be confirmed from **Fig. 12 (a)** before the density jump: $k_{//}=0.3$ cm^{-1} (nearly the same value with the fundamental antenna excited wave number $k_{//a}$) with the low ω_p value. In addition, a preliminary measurement of the excited magnetic fields at $z=23$ cm show different radial profiles between cases before and after the density jump.

Considering the present experimental conditions, only the whistler wave can propagate into the plasma. This wave, *i. e.*, R wave, can be expressed approximately as $k_{//}^2 = \omega \omega_p^2 \cos\theta / \omega_{ce} c^2$ (ω: excited RF angular frequency, ω_{ce}: electron cyclotron angular frequency, c: light velocity, θ : propagation angle with respect to the axial magnetic field) without imposing boundary conditions. Even though we take $\theta = 0°$ (parallel direction), the dispersion relation for the R wave at $t = 0.13$ ms and 0.25 ms is not satisfied: the experimental ω_p value is smaller by a factor of several times.

After the jump as shown in **Fig. 11**, this relation holds good for both inside and outside antenna regions. For the $m = -1$ case, $k_{//}$ value at the inside region is higher than that at the outside one, and ω_p value is somewhat smaller at the early plase after the density jump (for reference, $k_{//}$ value at $t = 0.13$ ms is nearly the same value expected from the R wave with $\theta < 10°$, discussed above). The time to satisfy this dispersion relation of the helicon wave is faster at the inside of the antenna region than that at the outside region, because of the faster density rise at the inside region. Note that a observed wave number after the jump is not decided by the antenna ($k_{//}a$) but by the plasma, *i.e.*, dispersion relation. These features before and after the density jump are also confirmed for the $B_0 = 0.5$ kG case.

Now, we discuss the errors in the experiment and calculation, because these errors are important to have an agreement between theoretical and experimental results quantitatively. As for the experiments, the error in the plasma density in total is less than 20%, which means less than 10% relative error in estimating ω_p value. This n_e error comes from a calibration of the absolute value, a reproducibility and plasma perturbation by the Langmuir probe, *i. e.*, n_e becomes somewhat lower ($< 15\%$) for the deep probe insertion case. The error in the $k_{//}$ value due to the averaging, reproducibility and perturbation, measured by magnetic probes is also considered to be less than 20%.

In the calculation, the increase in the ω_p value for the fixed $k_{//}$ value is estimated to be less than 15 % if we take another azimuthal mode number such as $m = 0$ mode in place of $m = 1$ or -1 modes; Preliminary wave measurement indicates that a normalized $m = 0$ mode amplitude is less than 20% after the plasma establishment, which means less than 3% error in the ω_p estimation. The effect of the second radial mode is also considered to be small. Although a wall radius effect is negligible (< 10 %)[4], a density profile effect for the $m = -1$ case is large (profile effect is negligible for the $m = 1$ case). According to a calculation from Refs. 4 and 5, a peaking of the density profile from the uniform to the parabolic profiles lowers the ω_p value by $\leq$ two times for the same $k_{//}$ value, which shows that the expected calculation curves in **Fig. 11 (b)** become more close to the experimental values. Therefore, the above mentioned conclusions need not to be altered from this discussion.

Figure 12 shows typical wave patterns along the z axis for the $m = 1$ excitation before the density jump of $t = 0.03$ ms and after of $t = 1.8$ ms ($P_{inp} = 1.2$ kW). Here, perpendicular components of the excited magnetic field at the plasma center ($r = 0$ cm) are measured by the interferometric method with the use of the boxcar integrator (full width of the time window is ≤ 0.04 ms). Various curves represent the different plases $\Delta\phi$ between the excited wave and antenna current in one RF cycle of 7 MHz by the use of a phase shifter.

Before the jump, the excited wave is localized at the antenna region with a standing wave character: nodes and loops can be clearly seen regardless of the phase. After the jump, we can interpret that this wave propagates outwards to the right (positive z direction), considering the phase $\Delta\phi$ and wave patterns at the positive z position in **Fig. 12 (b)**. On the contrary, there still exists a standing wave at the inside antenna region (especially at the left region). The increase in the plasma boundary with time (see **Fig. 7 (a)**) causes the larger amplitude of the magnetic field with the wider excited region moving to the right. Nearly the same features are obtained for $m=-1$ excitation as well as by the signal of the excited parallel magnetic field component. However, the excited wave is more localized near the antenna (only exists at $z<20$ cm with a smaller amplitude) for $m=-1$ excitation than that for $m=1$ excitation after the density jump, since there may be a larger collisional damping due to the higher plasma density near the antenna (see **Fig. 7**).

Here, we consider the wave nature appeared in this experiment (**Fig. 12**). In the antenna region before the density jump (low plasma density), a wave, which does not satisfy the dispersion relation of the helicon wave, can be forced to have a wave number of $k_{//a}$ (antenna excited wave number) with a boundary near the left and right sides of the antenna: a standing wave can exist as shown in **Fig. 12 (a)**.

When the excited wave satisfies this dispersion relation after the density jump near the antenna region (not at the outside region), a wave with the $m=1$ mode can propagate to the right and $m=-1$ to the left, although a directivity may be not so good since the antenna length is comparable with the excited wavelength. If there is a boundary (this boundary may be determined by the plasma region) near the antenna and the amplitudes of both modes are the same, a standing wave can also exist (there may be a wall ($z=-35$ cm) reflecting effect at the left side of the antenna region). After the density jump also at the outside region, the plasma boundary moves to the right, and the excited wave can propagate to the right with a standing wave character partly near the antenna region (**Fig. 11 (b)**).

We can rule out the possibility that this wave after the jump, which is thought as a standing wave near the antenna discussed above, is composed of the fundamental and higher harmonics (integer n) wave numbers with the same amplitudes; If there is a harmonics component, the obtained $k_{//}$ value in appearance changes by a factor of $(n-1)/2$. Therefore, the excited wave does not satisfy the expected dispersion relation for the helicon wave shown in **Fig. 11**, as the real experimental $k_{//}$ values change by a factor of $2/(n-1)$ (fundamental component) and $2n/(n-1)$ (harmonics component). In addition, it is difficult to excite the fundamental and higher harmonics components only, omitting the counter propagating wave, and also difficult to explain the wave patterns at outside antenna regions on the left and right sides.

Finally, we discuss a mechanism of the high density plasma production (a sudden density jump) briefly from the experimental results. Before the density jump, near field effect (especially inductive field near the antenna) is important to have a low density plasma with an order of 10^{11} cm^{-3} and relatively higher electron temperature (**Fig. 8**): a plasma and excited wave fields, which do not satisfy the dispersion relation (**Fig. 11**), are localized near the antenna (**Figs. 7** and **11 (a)**). Here, a capacitive coupling effect seems to be small due to a slight change of the antenna inductance stated before. In contrast, for

the ICP (Inductively Coupled Plasma) case with the higher filling pressure and without the axial magnetic field, the capacitive coupling may exist before the density jump[13]. Before this jump in our experiment, plasma density n_e increases almost linearly with an increase in the input power P_{inp}, while the electron temperatue T_e remains higher (10－15 eV range) than that after the jump.

When the power P_{inp} (in other word, electric field) exceeds a threshold value of about 1 kW, plasma density n_e increases drastically like an avalanche (**Fig. 8**) due to a cooperation effect as the n_e increase accelerates the plasma loading resistance R_p, which leads to an increase in the net absorbed power P_{net} by the plasma. When the density becomes higher, the excited wave can propagate as a helicon wave (**Fig. 11**) from the antenna to the outer regions (**Fig. 12 (b)**) and the high density plasma is produced by the collisional and electron Landau damping (collisional damping is stronger than electron Landau damping from calculation, and experimental damping length is discussed in Ref. 3). However, detailed spatiotemporal measuremetns of plasma parameters and wave excited fields including the electric fields are further necessary to draw a definite conclusion to explain the observed phenomena.

6. Conclusions

Exciting $m=1$ and -1 helical modes, the dynamic behavior of a helicon wave produced plasma is investigated. When the input RF power P_{inp} is greater than about 1 kW (net RF power $P_{net}>0.4$ kW), the density jump with drastic increases in plasma loading resistance R_p and Ar II line intensity are observed. After the time of this jump, electron temperature T_e and Ar I line intensity become lower, whereas Ar II line intensity increases. The RF power dependence and time evolution of Ar II line intensity experimentally obtained are consistent with calculation results.

Time evolution of radial and axial profiles such as I_{is} (ion saturation current) shows different features between $m=1$ and -1 excitation; For $m=-1$ excitation, I_{is} is localized near the antenna (along the z axis) and peaked radial profile (n_e is also peaked) is observed. In contrast, a peak position of I_{is} moves axially outwards with time for $m=1$ excitation.

Before a density jump, the excited wave is localized near the antenna with a standing wave character, and a dispersion relation of the helicon wave is not satistied. After the jump, the excited wave propagates axially outwards and the dispersion relation of the helicon wave is confirmed in both of the outside and inside antenna regions.

Acknowledgement

We would like to thank Prof. S. -I. Itoh for critical reading of our manuscript. This work has bee partly supported by a Grant in Aid for Encouragement of Young Scientists, Interdisciplinary Graduate School of Engineering Sciences.

References

1) R. W. Boswell, Plasma Phys. Control. Fusion **26** (1984) 1147.
2) F. F. Chen, Plasma Phys. Control. Fusion **33** (1991) 339.

3) A. Komori, T. Shoji, K. Miyamoto, J. Kawai and Y. Kawai, Phys. Fluids **B3** (1991) 893.
4) T. Shoji, Y. Sakawa, S. Nakazawa, K. Kadota and T. Sato, Plasma Sources Sci. Technol. **2** (1993) 5.
5) F. F. Chen, M. J. Hsieh and M. Light, Plasma Sources Sci. Technol. **3** (1994) 49.
6) Y. Yasaka and Y. Hara, Jpn. J. Appl. Phys. **33** (1994) 5950.
7) T. Shoji, private communication (1994).
8) P. Zhu and R. W. Boswell, Phys. Fluids **B3** (1991) 869.
9) V. Petržílka, Research Report IPPCZ-333, Institute of Plasma Physics, Czechoslovak Academy of Sciences (1993).
10) S. Shinohara, N. Asakura, M. Naito and K. Miyamoto, J. Phys. Soc. Jpn. **53** (1984) 1746.
11) S. Shinohara, O. Naito and K. Miyamoto, Nucl. Fusion **26** (1986) 1097.
12) S. Shinohara, O. Naito and K. Miyamoto, J. Phys. Soc. Jpn. **57** (1988) 665.
13) J. Amorim, H. S. Maciel and J. P. Sudano, J. Vac. Sci. Technol. **B9** (1991) 363.